EXPERIMENTAL STUDY OF THE COMPRESSIVE BEHAVIOR OF ENCELADUS AND EUROPA ICY PLUME DEPOSIT ANALOGS. E. Marteau[1], M. Choukroun[1], J. L. Molaro[1,2], E. Comstock[1], M. Gori[1], R. Hodyss[1], A. Murdza[3], E. Schulson[3], and X. Velez-Soto[1,4]; [1]Jet Propulsion Laboratory, California Institute of Technology, Pasadena, CA (eloise.marteau@jpl.nasa.gov); [2]Planetary Science Institute, Tucson, AZ, USA; [3]Dartmouth College, Hanover, NH, USA; [4]University of Puerto Rico Mayaguez, Mayaguez, PR, USA;

Introduction Potentially habitable icy Ocean Worlds, such as Enceladus and Europa, are scientifically compelling bodies and key targets in the robotic exploration of the solar system. Enceladus, and tentatively Europa, have a unique present-day activity that manifests itself through water-rich plumes ejecting materials from their internal habitable ocean onto their surfaces [1]. Plume deposits are expected to consist of fine-grained ice particles that evolve via sintering, possibly transforming initially unconsolidated deposits into consolidated porous ice [2,3]. The sintering phenomenon leads to the growth of the inter-particle necks and aggregate densification, resulting in the material as a whole becoming stronger over time [2,3]. Future robotic exploration of Enceladus and Europa by an in-situ mission would require a detailed understanding of the surface material properties and of the complex lander-surface interactions.

Recent research has shed lights into the mechanical properties of fine-grained plume deposits upon sintering [4,5,6]. A recent laboratory study examined the evolution in mechanical resistance of fine-grained ice particles using cone penetration measurements [4]. The results provided insights into the expected state of consolidation of plume deposits as a function of location and age on Enceladus and Europa. However, to date, a fundamental understanding of the mechanical behavior of icy plume deposits under Enceladus and Europa's surface conditions is largely lacking.

This work aims to explore the unconfined compressive behavior of icy plume deposits and its evolution upon sintering. Compressive tests are performed to derive the unconfined compressive strength of the material at different sintering stages, and to investigate its deformation and fracture behaviors. This work also discusses experimental techniques for studying the microstructure of ice plume deposits upon sintering, including particle size distribution, particle shape, and packing arrangement.

Ice plume deposit analogs preparation To create a laboratory analog of the ice plume deposits, deionized liquid water is sprayed into liquid nitrogen-filled container using an atomizing nozzle (Spraying Systems, Co). The water droplets instantly crystallize and form ice spherules. This fine-grained ice is stored in sealed containers or cylindrical molds and left to sinter at different temperatures, ranging from 193K to 243K, for up to 152 days. The starting ice particles are characterized by a log-normal size distribution with a median diameter of 12 μm. The samples exhibit a porosity of 51.5% ± 1.6%, with no discernable change for the duration of our experiments.

Custom-designed molds allow ice plume deposit samples to sinter. The cylindrical samples are then extracted from the molds and the evolution of their unconfined compressive strength over time is assessed. The samples have a diameter of 17.5 mm and an aspect ratio between 2.0 and 2.4.

Ice plume deposit analogs compressive behavior

Method. The compressive behavior of sintered ice samples is investigated with an Instron 5848 Microtester system equipped with a liquid nitrogen–cooled environmental chamber and a load cell of 2 kN load capacity. Tests are performed at 233 K. Teflon sheets are placed on the platens to limit frictional restraint between the icy samples and the platens. Compression tests are performed on each specimen by first applying a seating stress of approximately 0.1 MPa for 30 min to ensure positive contact between the specimen and platens. The specimen are then uniaxially loaded at a constant velocity of 1 mm/min, corresponding to strain rate ranging from 4.1×10^{-4} s^{-1} to 4.7×10^{-4} s^{-1} depending on the samples aspect ratio.

Results. Figures 1 and 2 show the stress-strain behavior of samples S1 and S2 that sintered, respectively, for 35 days at 193 K and 152 days at 243 K. In Figure 1, the engineering stress-strain curve of sample S1 exhibits three distinct regions: a linear elastic region up to small strains (~ 0.5%), strain hardening and densification. In the elastic regime, the slope of the stress-strain curve characterizes the Young's modulus E while the yield strength σ_Y correspond to the stress at which the material begins to deform plastically (i.e., at the onset of the plateau

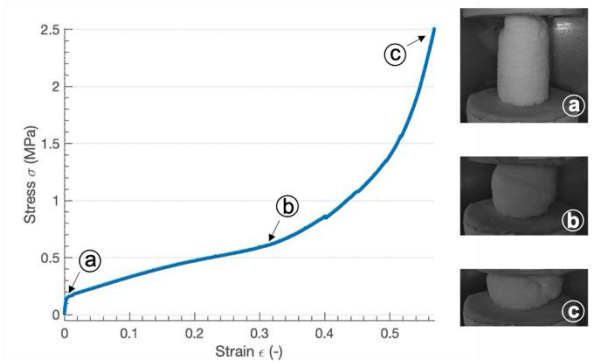

Figure 1: Stress-strain curve for sample S1 subjected to unconfined compression

regime). For sample S1, we have the Young's modulus E = 43.3 MPa and the yield strength σ_Y = 0.15 MPa. As the load increases, the pores begin to collapse and plastic strain is accumulated at a roughly constant load. A further increase in load leads to densification, which causes the load to increase rapidly without a significant increase in strain.

In contrast to sample S1 which displays ductile behavior, sample S2 exhibits brittle characteristics. Sample S2 was left to sinter for a longer period of time than sample S1 and at a warmer temperature. As illustrated in Figure 2, deformation of sample S2 proceeds by brittle fracture along several cracks, leading to the major drops in the stress-strain curve. The compressive stress applied on sample S2 reaches a maximum value of 0.35 MPa.

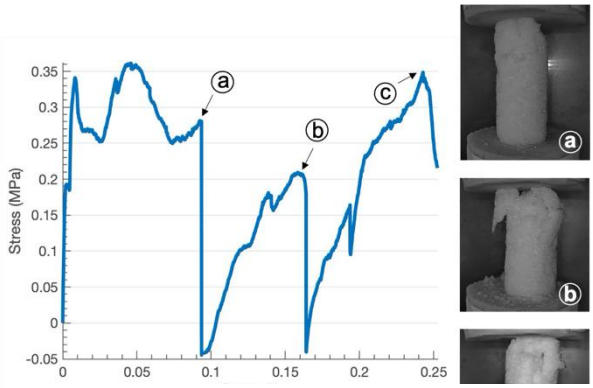

Figure 2: Stress-strain curve for sample S2 subjected to unconfined compression

Discussion After sintering 35 days at 193 K, Choukroun et al. [4] report a cone penetration resistance of sintered ice samples in the order of 0.5-1 MPa, which is commensurate to the compressive stresses applied to sample S1 as reported in Figure 1. While cone penetration resistance cannot be directly compared to compressive strength, both properties provide general insight on the envelop of strength characteristics the material exhibit. Sample S2 fails in compression at much lower stresses than the expected cone penetration resistance of ~ 20 MPa for a sample that sintered 152 days at 243 K. As illustrated in Figure 2, the compressive failure of sample S2 is mostly localized at the contact region with the top platen, which likely occurs due to an imperfect specimen/platen bedding. Future investigations are needed to assess the repeatability of compression strength measurements at different sintering stages and to further characterize the relationship between cone penetration resistance and compressive strength.

Microstructure characterization Cryogenic optical microscopy is conducted with an Olympus BX51 microscope equipped with a Linkam LTS350 cryostage. A small fraction of the sample is scraped off the walls (at depth) at CPT test locations and transferred cold (~ 173 K) into the cryostage for analysis. The Olympus Stream software and custom Matlab routines enable batch-processing and analysis of the images to extract particle size distribution information. X-ray microcomputed tomography of the samples is conducted under cold conditions at Dartmouth College's Ice Research Laboratory to investigate the distribution of porosity and the packing arrangement of ice particles within the samples. Recent works show that an increase in particle size and particle contact area occur with sintering time [2,3]. Detailed microscopic analysis of different states of sintered microstructure will provide insight into how changes in packing arrangement and aggregate formation influence mechanical properties, such as Young's modulus and compressive strength.

Acknowledgments Part of this work has been conducted at the Jet Propulsion Laboratory, California Institute of Technology, under contract to NASA. Support from the JPL Research and Technology Development Program is acknowledged. Government sponsorship acknowledged.

References [1] Porco et al. (2006) *Science*, 311(5766). [2] Molaro et al. (2019) *J. Geophys. Res. Planets*, 124(2). [3] Blackford (2007) *J. Phys. D: Appl. Phys*, 40(21). [4] Choukroun et al. (2020) *GRL*, 47(15). [5] Choukroun et al. (2021) *Planet. Sci. J*, 2(100). [6] Dhaouadi et al. (2022) *Granul. Matter*, 24(1).